Supplement of Atmos. Chem. Phys., 20, 2719–2734, 2020
https://doi.org/10.5194/acp-20-2719-2020-supplement

Atmospheric Chemistry and Physics
Open Access

Supplement of

Effect of ammonia on fine-particle pH in agricultural regions of China: comparison between urban and rural sites

Shenbo Wang et al.

Correspondence to: Shasha Yin (shashayin@zzu.edu.cn) and Ruiqin Zhang (rqzhang@zzu.edu.cn)

Text S1 Calculation of ions balance and equivalent ratio.

The ions balance and equivalent ratio are calculated using the following formulas:

$$[\mathrm{cations}] = \frac{[\mathrm{NH_4^+}]}{18} + \frac{[\mathrm{Na^+}]}{23} + \frac{[\mathrm{K^+}]}{39} + \frac{[\mathrm{Ca^{2+}}]}{20} + \frac{[\mathrm{Mg^{2+}}]}{12} \quad (1)$$

$$[\mathrm{anions}] = \frac{[\mathrm{SO_4^{2-}}]}{48} + \frac{[\mathrm{NO_3^-}]}{62} + \frac{[\mathrm{Cl^-}]}{35.5} \quad (2)$$

$$\mathrm{ion\ balance} = [\mathrm{cations}] - [\mathrm{anions}] \quad (3)$$

$$\mathrm{equivalent\ ratio} = [\mathrm{cations}]/[\mathrm{anions}] \quad (4)$$

where $[Na^+]$, $[K^+]$, $[Ca^{2+}]$, $[Mg^{2+}]$, $[NH_4^+]$, $[SO_4^{2-}]$, $[NO_3^-]$, and $[Cl^-]$ are the measured concentrations (μg/m^3) in the atmosphere. In addition to the measurement uncertainties, equivalent ratios lower than 1 might be attributed to the loss of cations from the volatilization of ammonium and unmeasured hydrogen ions (Meng et al., 2016). Equivalent ratios higher than 1 were most likely caused by water-soluble organic anions, CO_3^{2-} and HCO_3^- contents that were not detected in chemical analysis (Tian et al., 2018).

Text S2 Backward trajectory frequency analysis

The Hybrid Single-Particle Lagrangian Integrated Trajectory (HYSPLIT) Web version of the National Oceanic and Atmospheric Administration Air Resources Laboratory (Stein et al., 2015) was used to calculate backward trajectories from gridded meteorological data (at 500 m above ground level) at regular time intervals (12 h). For modeling the trajectory frequency, the system will start a trajectory from a single location and height every 6 hours and then sum the frequency that the trajectory passed over a grid cell and then normalize by either the total number of trajectories or endpoints. The grid resolution was selected as 1° according to the scale of the desired result. The frequency distribution maps (Fig. S7) of the five sampling sites recorded during the three cases support our findings: the southern regions of Henan Province (e.g., Xuchang and Zhumadian cities) were a high probability (> 20 %) source for the five sites during Case 1 (Fig. S7a); the trajectory frequency during Case 2 (Fig. S7b) uniformly distributed around the receptor sites is most probably connected to local emissions; and the five sites during Case 3 (Fig. S7c) were affected by the air masses from northeastern areas (e.g., Dezhou and Liaocheng cities) with the frequencies higher than 20 %.

Text S3 NH_x calculation

With respect to measurements of semi-volatile gases, the concentrations of NH_3 were extremely higher than HNO_3 and HCl, consistent with the Song et al. (2018) and Liu et al. (2017). TNHx, required NHx (Required-NHx), and excess NHx (Excess-NHx) concentrations were calculated using the following formulas:

$$\text{Total NH}_x = 17 \times \left(\frac{[\text{NH}_4^+]}{18} + \frac{[\text{NH}_3]}{17}\right), \tag{5}$$

$$\text{Required NH}_x = 17 \times \left(\frac{[SO_4^{2-}]}{48} + \frac{[NO_3^-]}{63} + \frac{[Cl^-]}{35.5} + \frac{[HNO_3]}{64} + \frac{[HCl]}{36.5}\right) - 17 \times \left(\frac{[Na^+]}{23} + \frac{[K^+]}{39} + \frac{[Ca^{2+}]}{20} + \frac{[Mg^{2+}]}{12}\right), \quad (6)$$

$$\text{Excess NH}_x = \text{total NH}_x - \text{required NH}_x, \quad (7)$$

where $[Na^+]$, $[K^+]$, $[Ca^{2+}]$, $[Mg^{2+}]$, $[NH_4^+]$, $[SO_4^{2-}]$, $[NO_3^-]$, $[Cl^-]$, $[NH_3]$, $[HNO_3]$, and $[HCl]$ are the measured mass concentrations (μg/m^3) of these species. Excess-NH_x in this study represents a part of TNH_x (gas NH_3 + particle NH_4^+), while the other NH_x plus nonvolatile cations have been equivalent to all anions (Blanchard et al., 2000). If Excess-NH_x is above 0, then the system is considered NH_x-rich. Otherwise, the system is under the NH_x-poor condition.

Figure lists:

Fig. S1 Locations of the five monitoring stations in Henan Province, China (i.e., urban sites at Zhengzhou (U-ZZ) and Anyang (U-AY), rural sites at Anyang (R-AY), Xinxiang (R-XX), and Puyang (R-PY)). © 2019 National Geomatics Center of China. All rights reserved.

Fig. S2 Comparison between the predicted and measured NH_4^+, NO_3^-, Cl^-, NH_3, HNO_3 and HCl at the five sites.

Fig. S3 Ion balance of water-soluble inorganic ions at the five sites.

Fig. S4 Comparison between the predicted and input NH_4^+ (a, d) and NH_3 (b, c) concentrations, the original and adjusted pH (c, f) of U-ZZ and R-PY sites after adjusting the measured NH_4^+ concentrations to fit the ion balance.

Fig. S5 Comparison of predicted pH by ISORROPIA-II with E-AIM IV at the U-ZZ site.

Fig. S6 Temporal variations of temperature (T), relative humidity (RH), wind speed (WS), wind direction (WD), and concentrations of NH_3, NH_4^+, SO_4^{2-}, and NO_3^- during three cases at U-AY (a), R-

AY (b), R-XX (c), and R-PY (d) sites. The shaded areas represent the measurement uncertainties.

Fig. S7 Trajectory frequencies of typical periods at the five sites during Cases 1(a), 2(b), and 3(c). The color scale bar represents the percentage of trajectories passing through each grid to total trajectories.

Fig. S8 Time series of predicted $PM_{2.5}$ pH at the five sites. The shaded areas show the range of uncertainty in pH for the pH_{max} and pH_{min} calculations.

Fig. S9 Correlations between pH and H^{+}_{air} during sampling periods at the five sites. The color scale bar represents the aerosol water content (AWC) concentration.

Fig. S10 Sensitivity tests of $PM_{2.5}$ pH to input data. The real-time measured values of a variable and the average values of other parameters during Case 2 were input into the ISORROPIA II model.

Fig. S11 Comparisons of the sensitivities of $PM_{2.5}$ pH to TNa, K^{+}, Ca^{2+}, and Mg^{2+} among the five sites. The color scale bar represents the pH values. The relative standard deviation (RSD) and range (Range) represent the sensitivity degree of pH to this variable and range (min–max) of the re-predicted pH value in the test, respectively.

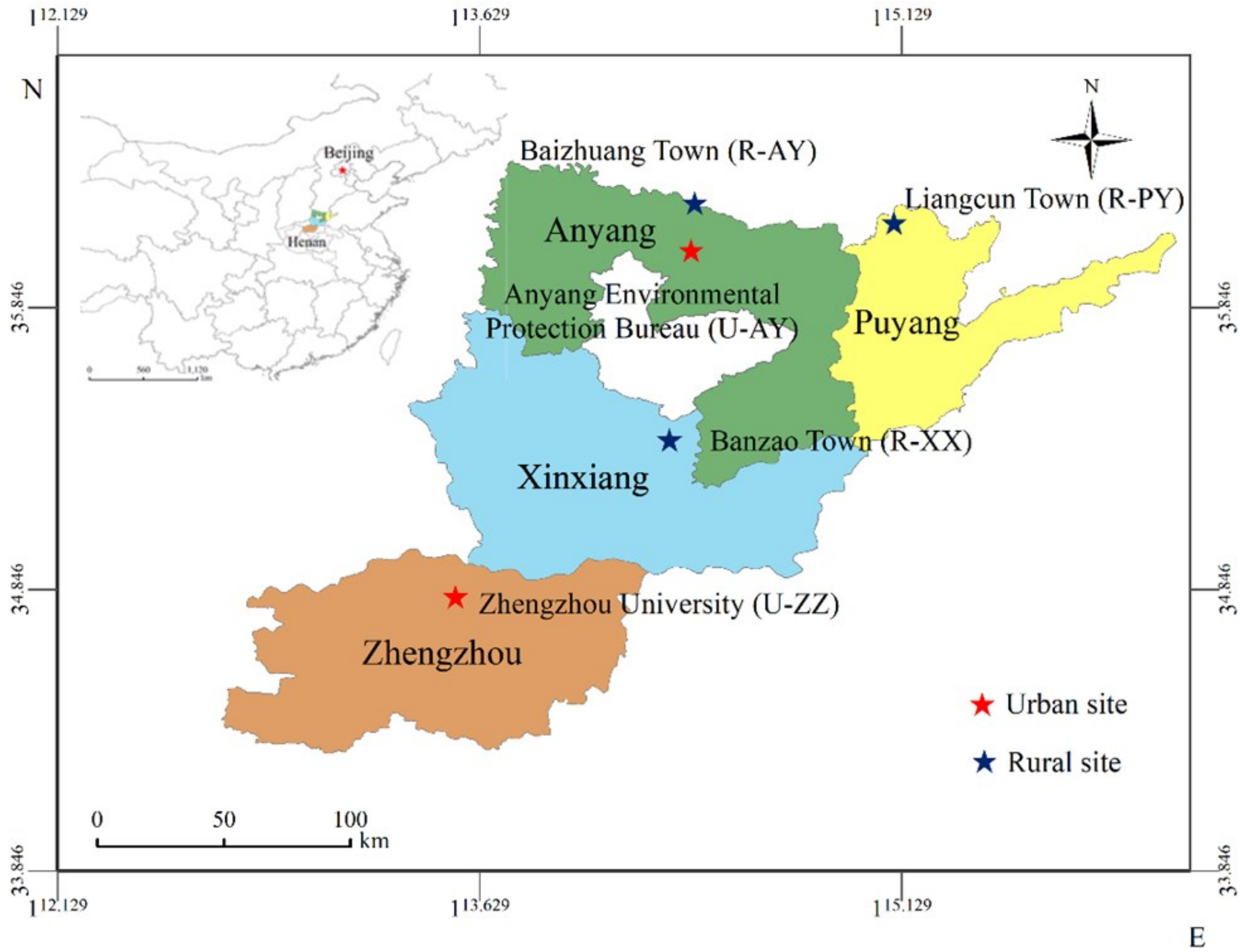

Fig. S1 Locations of the five monitoring stations in Henan Province, China (i.e., urban sites at Zhengzhou (U-ZZ) and Anyang (U-AY), rural sites at Anyang (R-AY), Xinxiang (R-XX), and Puyang (R-PY)).

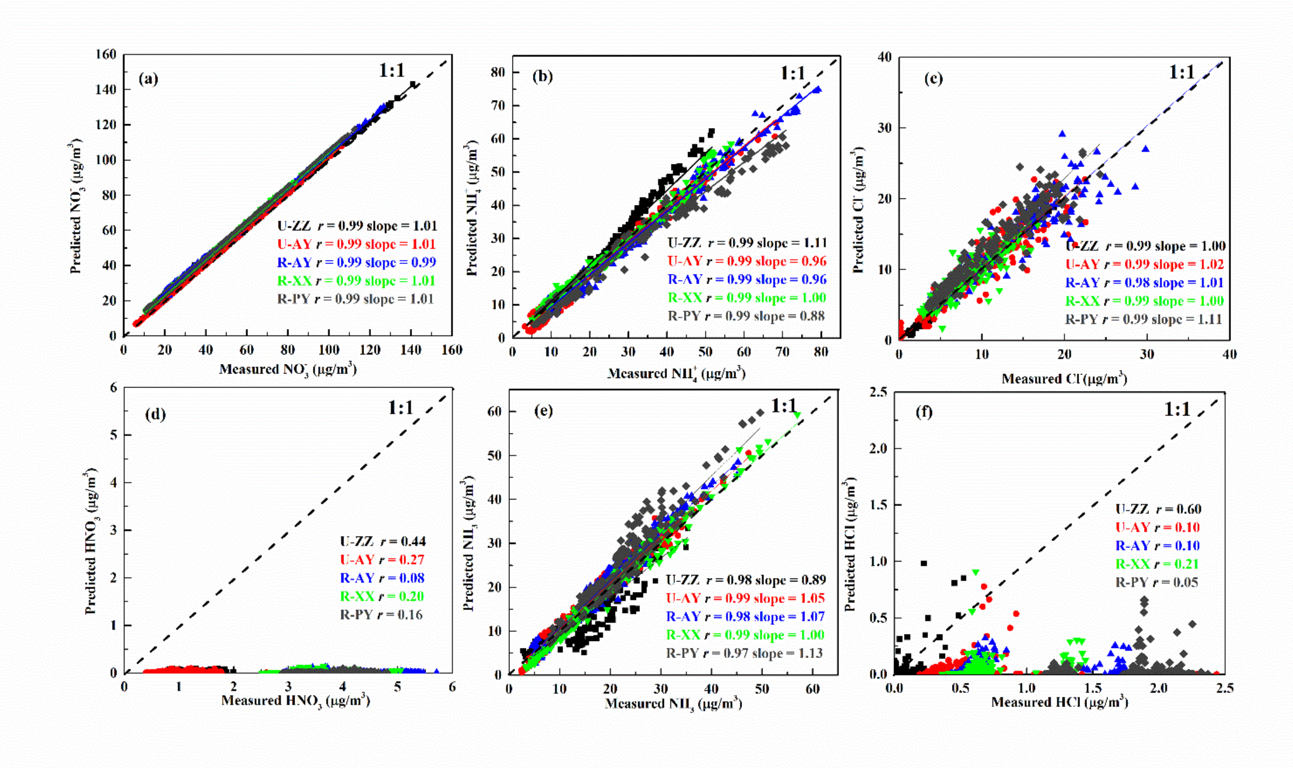

Fig. S2 Comparison between the predicted and measured NH_4^+, NO_3^-, Cl^-, NH_3, HNO_3 and HCl at the five sites.

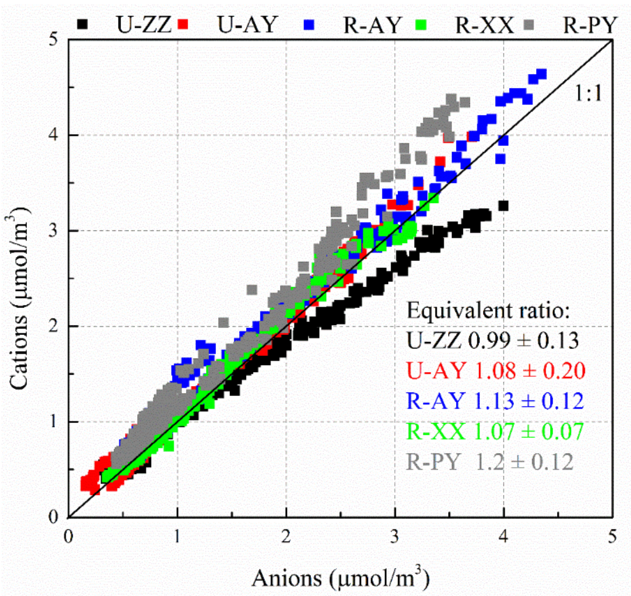

Fig. S3 Ion balance of water-soluble inorganic ions at the five sites.

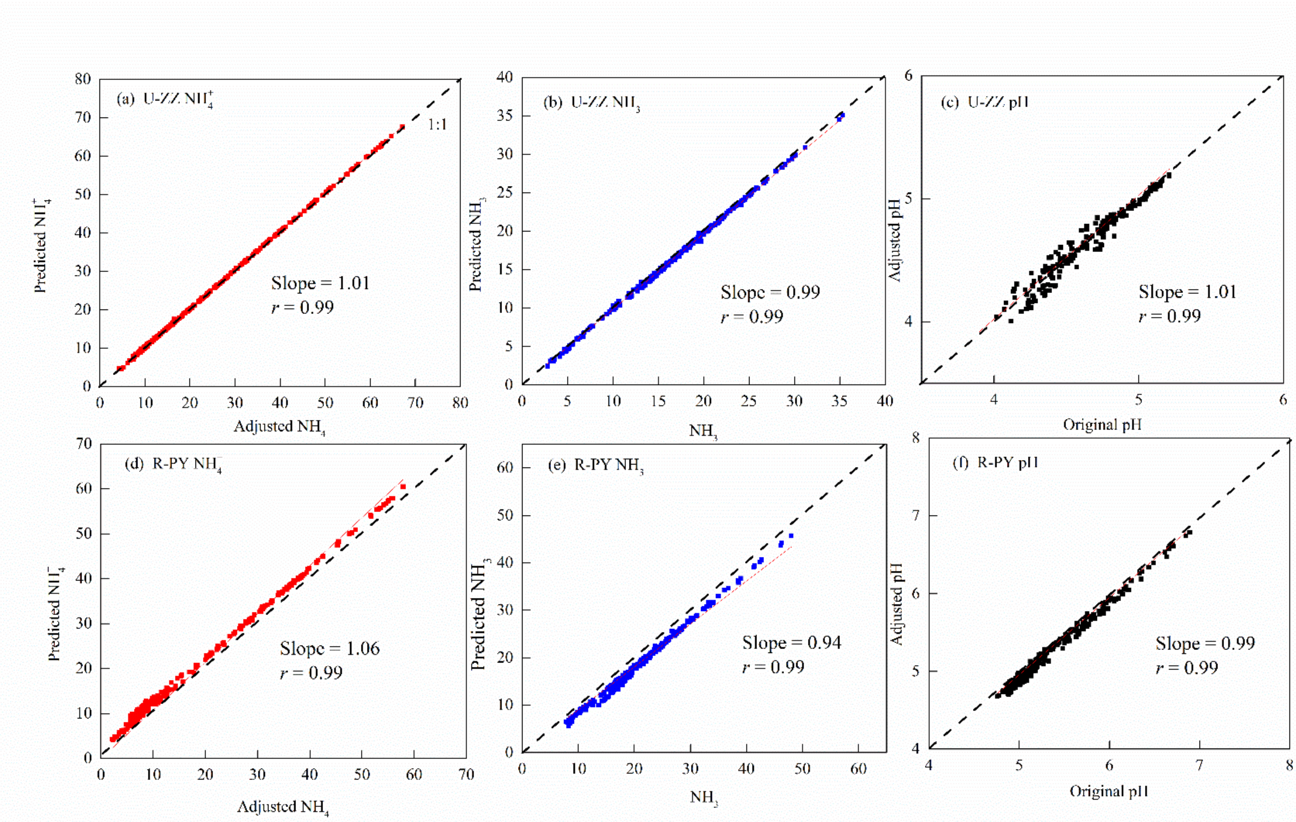

Fig. S4 Comparison between the predicted and input NH_4^+ (a, d) and NH_3 (b, c) concentrations, the original and adjusted pH (c, f) of U-ZZ and R-PY sites after adjusting the measured NH_4^+ concentrations to fit the ion balance.

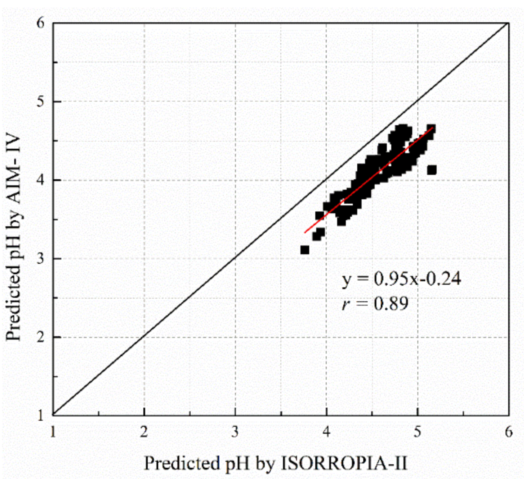

Fig. S5 Comparison of predicted pH by ISORROPIA-II with E-AIM IV at the U-ZZ site.

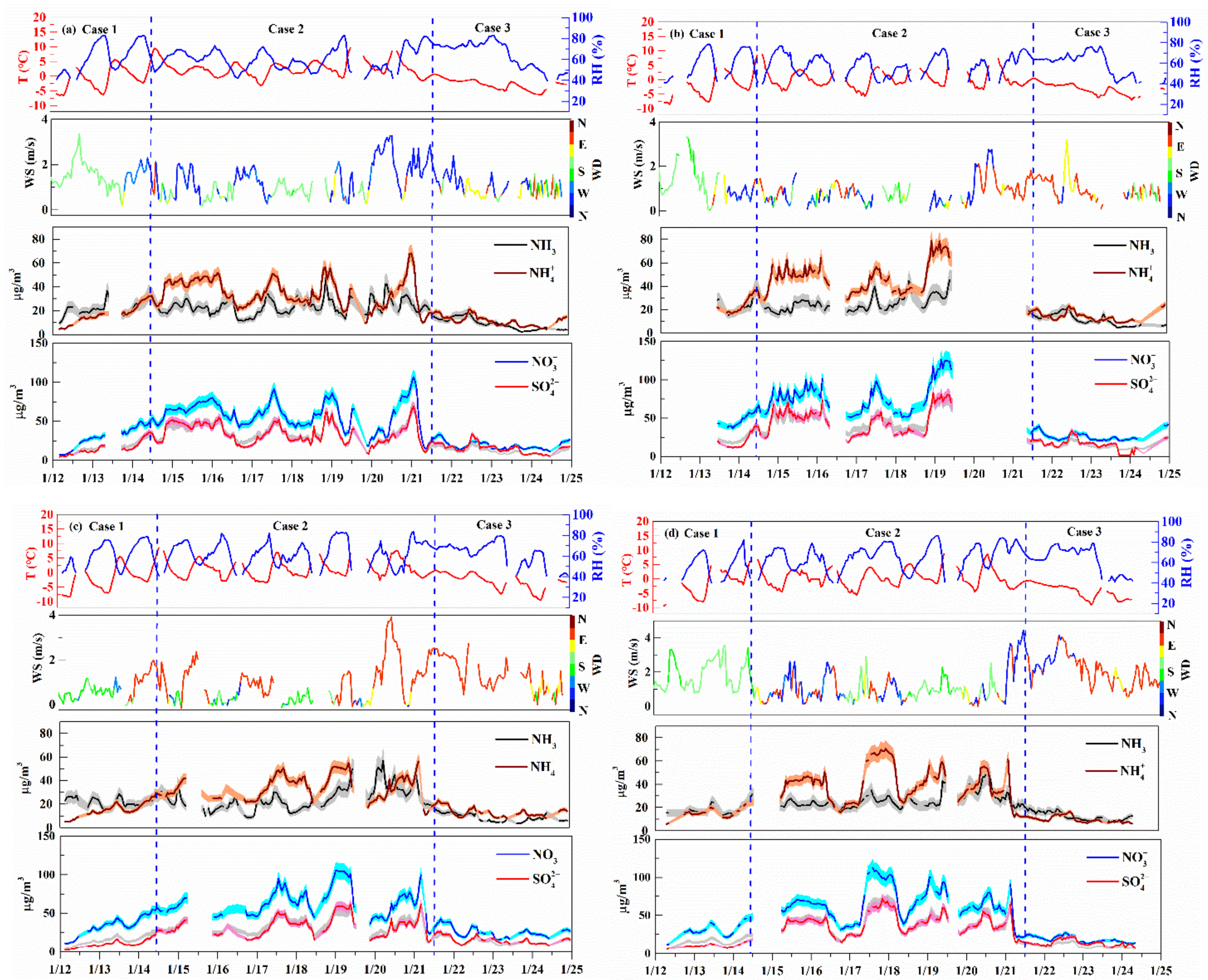

Fig. S6 Temporal variations of temperature (T), relative humidity (RH), wind speed (WS), wind direction (WD), and concentrations of NH_3, NH_4^+, SO_4^{2-}, and NO_3^- during three cases at U-AY (a), R-AY (b), R-XX (c), and R-PY (d) sites. The shaded areas represent the measurement uncertainties.

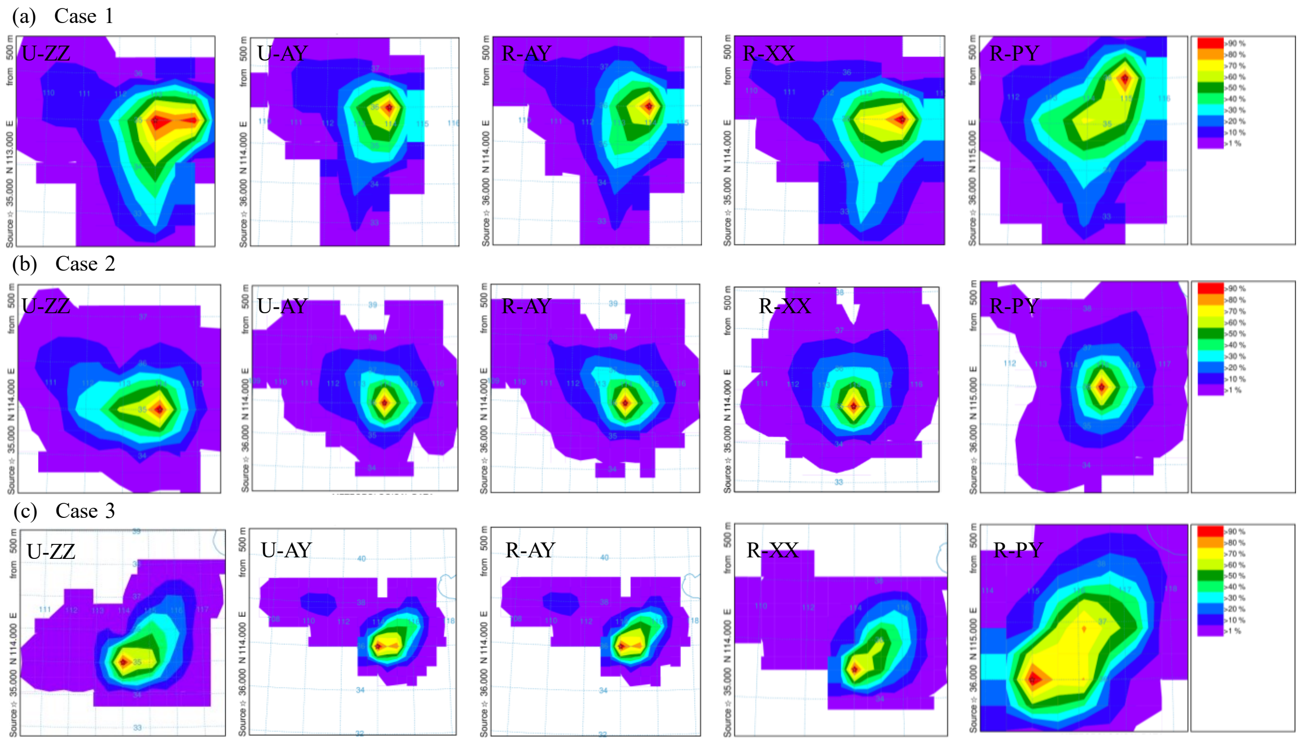

Fig. S7 Trajectory frequencies of typical periods at the five sites during Cases 1(a), 2(b), and 3(c). The color scale bar represents the percentage of trajectories passing through each grid to total trajectories.

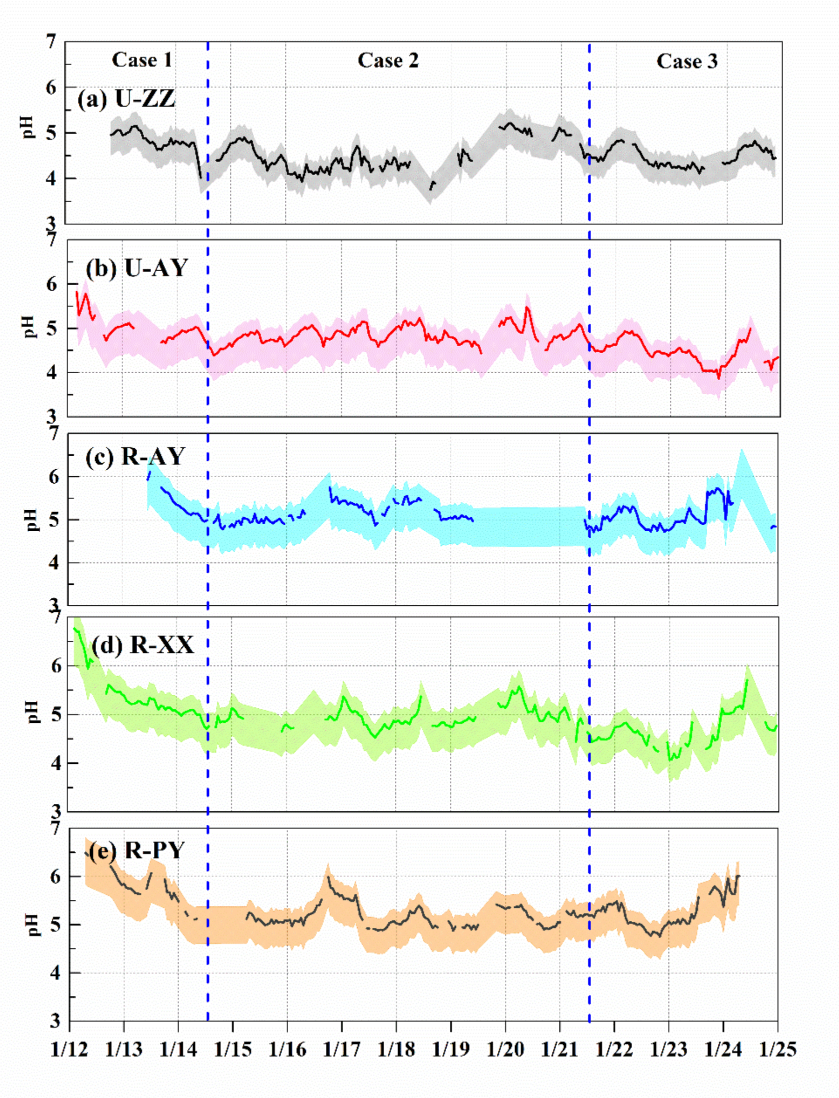

Fig. S8 Time series of predicted $PM_{2.5}$ pH at the five sites. The shaded areas show the range of uncertainty in pH for the pH_{max} and pH_{min} calculations.

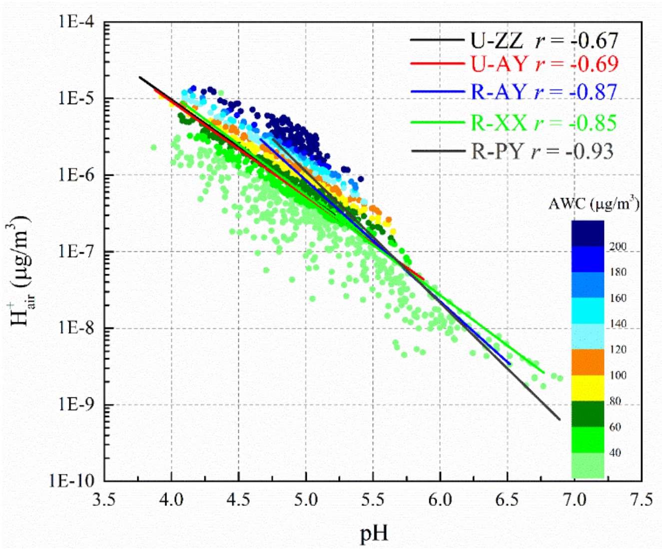

Fig. S9 Correlations between pH and H^+_{air} during sampling periods at the five sites. The color scale bar represents the aerosol water content (AWC) concentration.

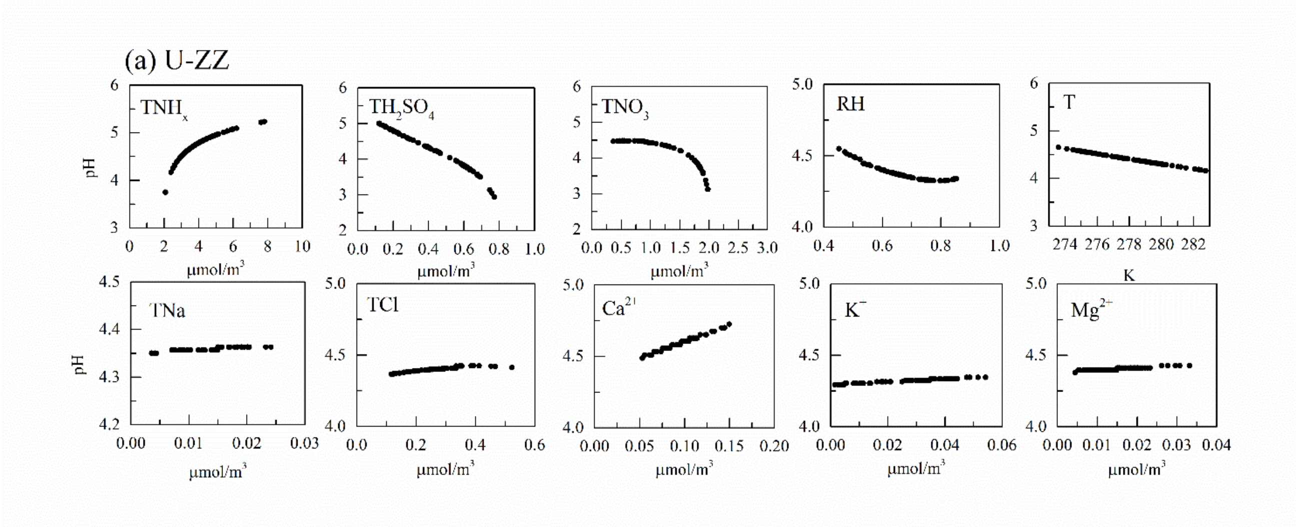

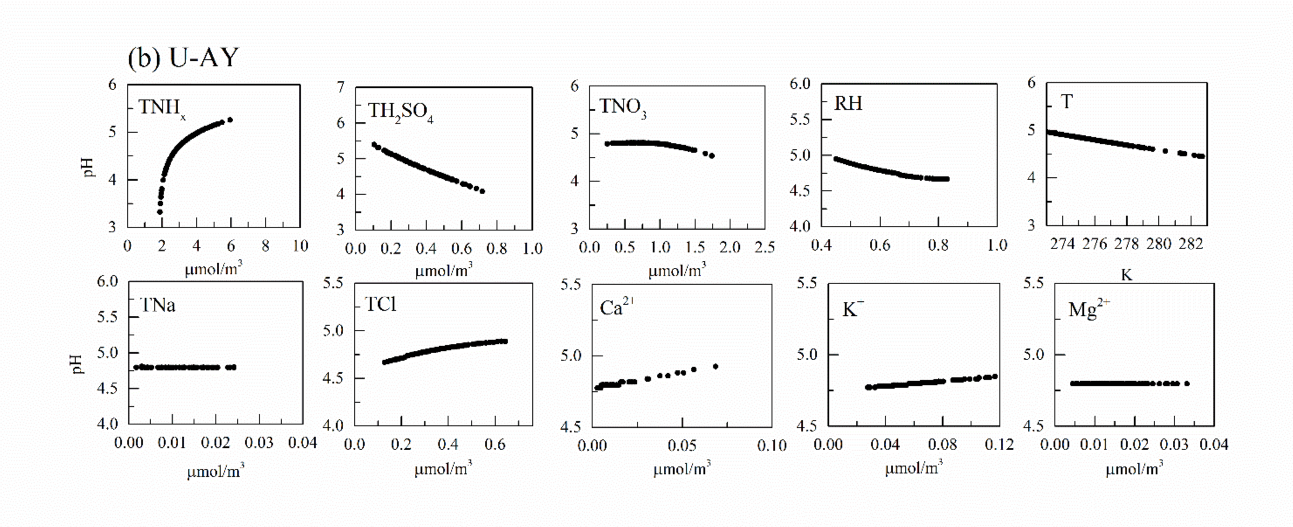
(b) U-AY
TNH$_x$
TH$_2$SO$_4$
TNO$_3$
RH
T
TNa
TCl
Ca^{2+}
K$^+$
Mg^{2+}
pH
μmol/m^3
K

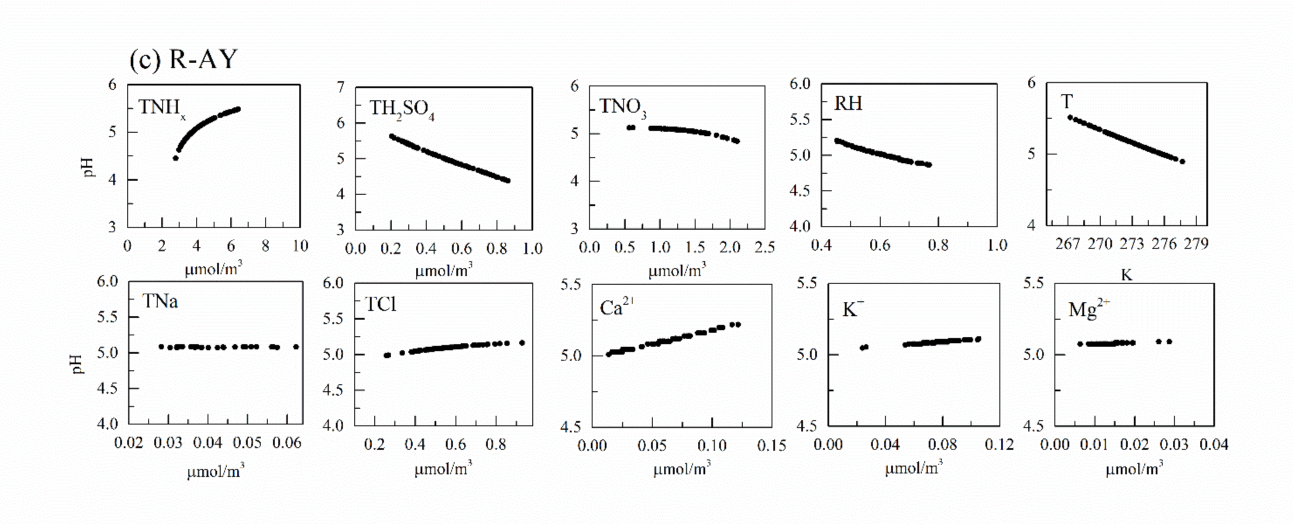
(c) R-AY
TNH$_x$
TH$_2$SO$_4$
TNO$_3$
RH
T
TNa
TCl
Ca^{2+}
K$^+$
Mg^{2+}
pH
μmol/m^3
K

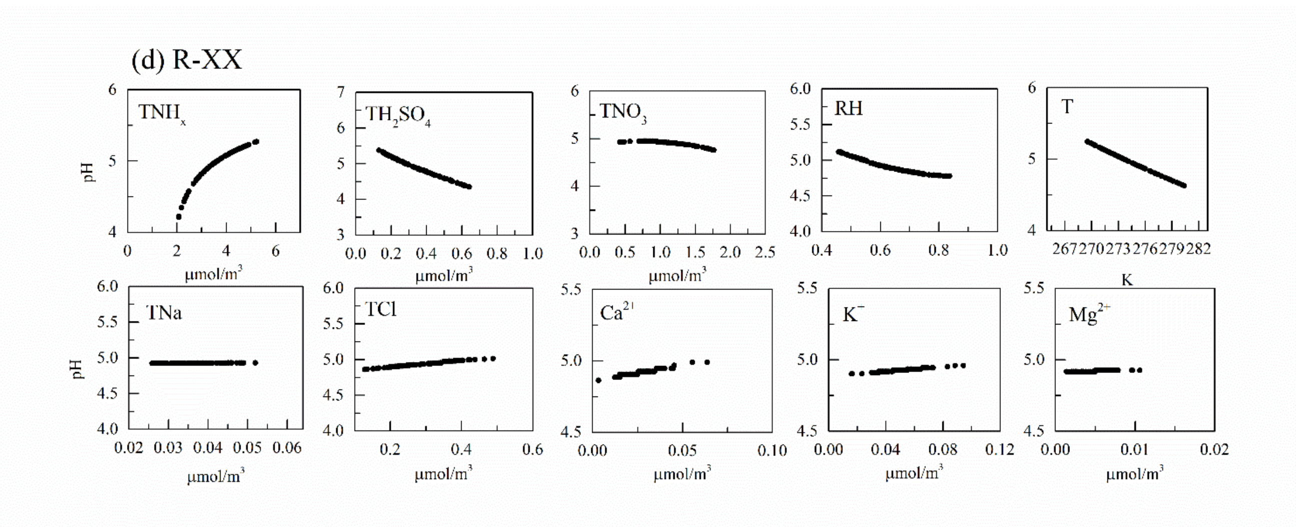
(d) R-XX
TNH$_x$
TH$_2$SO$_4$
TNO$_3$
RH
T
TNa
TCl
Ca^{2+}
K$^+$
Mg^{2+}
pH
μmol/m^3
K

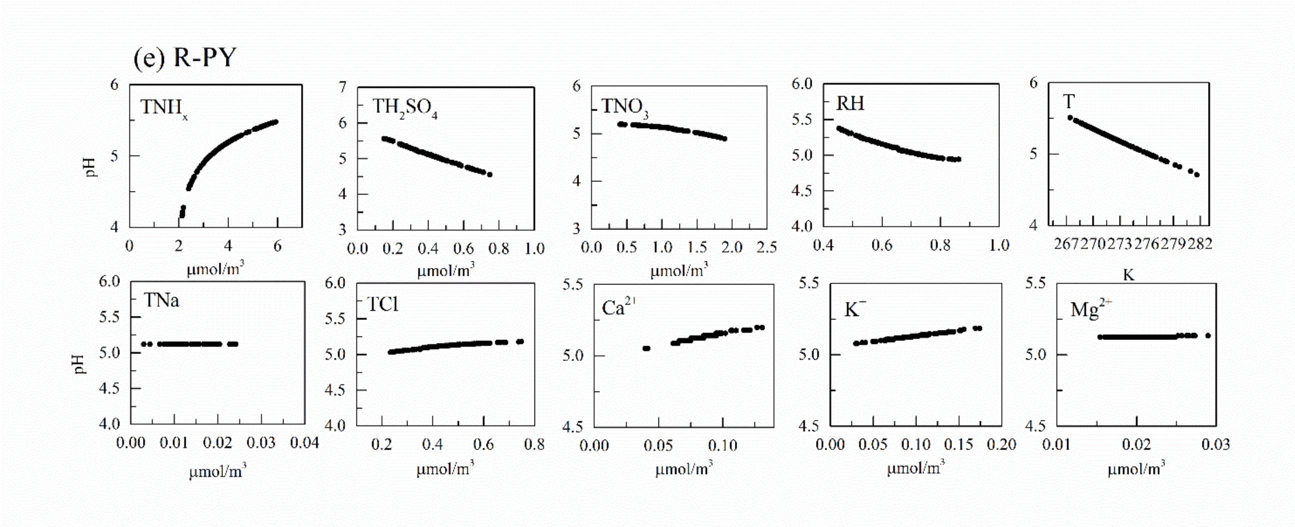

Fig. S10 Sensitivity tests of $PM_{2.5}$ pH to input data. The real-time measured values of a variable and the average values of other parameters during Case 2 were input into the ISORROPIA II model.

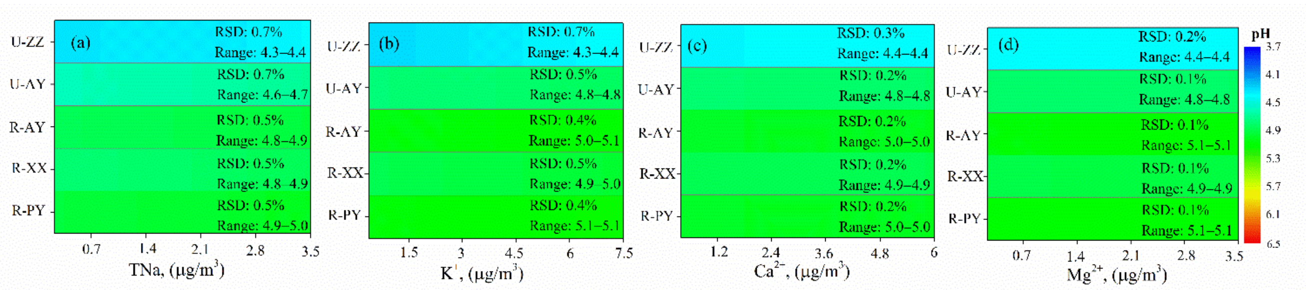

Fig. S11 Comparisons of the sensitivities of $PM_{2.5}$ pH to TNa (replaced by observed Na^+), K^+, Ca^{2+}, and Mg^{2+} among the five sites. The color scale bar represents the pH values. The relative standard deviation (RSD) and range (Range) represent the sensitivity degree of pH to this variable and range (min–max) of the re-predicted pH value in the test, respectively.

Table lists:

Table S1 Summarized NH_3 concentrations ($\mu g/m^3$) in this study and other sites.

Table S2 Statistical values of pH during three cases.

Table S3 Pearson's correlation coefficients (*r*) between H^+_{air} with observed data at the five sites.

Table S4 Variation ranges of each variable for assessing the different effects of this variable among five sites and their observed minimum and maximum values.

Table S1 Summarized NH_3 concentrations ($\mu g/m^3$) in this study and other sites.

Cities	Period	NH_3	References
Zhengzhou, China	2018.01	22.0 ±8.9	This study
Anyang, China	2018.01	25.3 ± 10.5	This study
Anyang, China	2018.01	25.8 ± 12.0	This study
Xinxiang, China	2018.01	26.1 ± 14.0	This study
Puyang, China	2018.01	27.1 ± 17.3	This study
Zhengzhou, China	2017.03–2018.04	11.7	Wang et al., 2018
Beijing, China	2015.01–03	7.3	Zhang et al., 2018
Beijing, China	2008.02–2010.07	22.8 ± 16.3	Wang et al., 2018
Beijing, China	2007.01–2010.07	10.2 ± 10.8	Wang et al., 2018
Beijing, China	2001.07–2001.08	16.8–42.2	Wang et al., 2018
North China Plain, China	2006.08–2009.09	11.7–31.9	Shen et al., 2011
Xi'an, China	2006.04–2007.04	18.6	Wang et al., 2018
Xi'an, China	2006.04–2007.04	20.3	Wang et al., 2018
Chengdu, China	2014.07–2015.04	10.5 ± 4.8	Wang et al., 2016
Wanzhou, China	2014.07–2015.04	8.3 ± 4.7	Wang et al., 2016

shanghai, China	2014.05–2015.06	7.8	Chang et al., 2019
Hangzhou, China	2012.04–05	12.8	Jansen et al., 2014
Dalian, China	2010.09–2012.04	1.5	Luo et al., 2014
Fenghua, China	2010.08–2012.05	3.7	Luo et al., 2014
Fujian, China	2015.06–2016.05	21.0 ± 7.9	Wang et al., 2018
Fujian, China	2015.06–2017.03	10.5–13.5	Wu et al., 2018
Hong Kong, China	2003.10–2006.05	10.2	Tanner, 2009
Carolina, USA	2000.01–12	0.4–3.4	Walker et al., 2004
Delhi, India	2013.01–2015.12	25.3 ± 4.6	Saraswati et al., 2019

Table S2 Statistical values of pH during three cases.

	Case 1				Case 2				Case 3			
	25th percentile	Median	75th percentile	Average	25th percentile	Median	75th percentile	Average	25th percentile	Median	75th percentile	Average
U-ZZ	4.7	4.8	5.0	4.8	4.3	4.5	4.8	4.5	4.3	4.5	4.7	4.5
U-AY	4.8	5.0	5.2	5.1	4.7	4.8	5.0	4.8	4.4	4.5	4.8	4.5
R-AY	5.1	5.4	5.8	5.5	5.0	5.1	5.4	5.2	4.9	5.0	5.3	5.1
R-XX	5.1	5.3	5.6	5.4	4.8	4.9	5.1	4.9	4.5	4.7	5.0	4.7
R-PY	5.7	6.0	6.3	6.0	5.0	5.1	5.4	5.2	5.0	5.2	5.4	5.3

Table S3 Pearson's correlation coefficients (*r*) between H^{+}_{air} with observed data at the five sites.

	U−ZZ	U−AY	R−AY	R−XX	R−PY
TWSIIs	0.834^{**}	0.521^{**}	0.676^{**}	0.530^{**}	0.774^{**}
TNH_x	0.650^{**}	0.368^{**}	0.544^{**}	0.301^{**}	0.703^{**}
TH_2SO_4	0.867^{**}	0.625^{**}	0.765^{**}	0.638^{**}	0.811^{**}
TNO_3	0.828^{**}	0.458^{**}	0.607^{**}	0.502^{**}	0.767^{**}
TCl	0.430^{**}	0.406^{**}	0.602^{**}	0.223^{**}	0.419^{**}
K^+	0.757^{**}	0.388^{**}	0.551^{**}	0.138^{*}	0.485^{**}
Ca^{2+}	-0.161^{*}	-0.234^{**}	-0.137^{*}	-0.248^{**}	0.06
TNa	0.306^{**}	−0.095	0.098	0.103	-0.138^{*}
Mg^{2+}	−0.009	−0.027	−0.018	−0.050	0.026
AWC	0.63^{**}	0.739^{**}	0.903^{**}	0.755^{**}	0.938^{**}
T	0.012	0.045	-0.138^{*}	−0.023	0.146^{*}
RH	0.337^{**}	0.610^{**}	0.631^{**}	0.637^{**}	0.658^{**}

* Correlation is significant at the 0.05 level (two-tailed).

** Correlation is significant at the 0.01 level (two-tailed).

Table S4 Variation ranges of each variable for assessing the different effects of this variable among five sites and their observed minimum and maximum values.

Species	Observation		Setting		Gradient
	Min	Max	Min	Max	
T (°C)	−5.8	14.3	−6	15	0.1
RH (%)	26.8	92.3	30	95	0.1
TNH_x (μg/m^3)	21.2	96.7	25	95	0.01 μmol/m^3
TNO_3 (μg/m^3)	5.8	132.6	1	125	0.01 μmol/m^3
TH_2SO_4 (μg/m^3)	6.9	82.7	10	80	0.01 μmol/m^3
TCl (μg/m^3)	0.54	39.5	0.35	35	0.01 μmol/m^3
TNa (μg/m^3)	0.29	3.33	0.25	3.5	0.01 μmol/m^3
K^+ (μg/m^3)	0.27	7.8	0.1	7.5	0.01 μmol/m^3
Ca^{2+} (μg/m^3)	0.2	5.2	0.4	6	0.01 μmol/m^3
Mg^{2+} (μg/m^3)	0.11	3.1	0.25	3.5	0.01 μmol/m^3

References:

Blanchard, C. L., P. M. Roth, S. J. Tanenbaum, S. D. Ziman, and J. H. Seinfeld: The use of ambient measurements to identify which precursor species limit aerosol nitrate formation, J. Air Waste Manage. Assoc., 50, 2073–2084, 2000.

Chang, Y., Zou, Z., Zhang, Y., Deng, C., Hu, J., Shi, Z., Dore, A. J., Collett, J. L.: Assessing contributions of agricultural and nonagricultural emissions to atmospheric ammonia in a Chinese megacity. Environ. Sci. Technol., 53, 1822–1833, 2019.

Jansen, R. C., Shi, Y., Chen, J., Hu, Y., Xu, C., Hong, S., Li, J., Zhang, M.: Using hourly measurements to explore the role of secondary inorganic aerosol in $PM_{2.5}$ during haze and fog in Hangzhou, China. Adv. Atmos. Sci., 31, 1427–1434, 2014.

Liu, M., Song, Y., Zhou, T., Xu, Z., Yan, C., Zheng, M., Wu, Z., Hu, M., Wu, Y., Zhu, T.: Fine particle pH during severe haze episodes in northern China. Geophys. Res. Lett., 44, 5213−5221, 2017.

Luo, X. S., Tang, A. H., Shi, K., Wu, L. H., Li, W. Q., Shi, W. Q., Shi, X. K., Erisman, J. W., Zhang, F., Liu, X. J.: Chinese coastal seas are facing heavy atmospheric nitrogen deposition. Environ. Res. Lett., 9, 095007, 2014.

Meng, C. C., Wang, L. T., Zhang, F. F., Wei, Z., Ma, S. M., Ma, J., Yang, J.: Characteristics of concentrations and water-soluble inorganic ions in $PM_{2.5}$ in Handan City, Hebei province, China. Atmos. Res., 171, 133−146, 2016.

Saraswati, Sharma, S. K., Saxena, M., Mandal, T. K.: Characteristics of gaseous and particulate ammonia and their role in the formation of secondary inorganic particulate matter at Delhi, India. Atmos. Res., 218, 34–49, 2019.

Shen, J., Liu, X., Ying, Z., Fangmeier, A., Goulding, K., Zhang, F.: Atmospheric ammonia and particulate ammonium from agricultural sources in the North China Plain. Atmos. Environ., 45, 5033–5041, 2011.

Song, S., Gao, M., Xu, W., Shao, J., Shi, G., Wang, S., Wang, Y., Sun, Y., Mcelroy, M. B.: Fine particle pH for Beijing winter haze as inferred from different thermodynamic equilibrium models. Atmos. Chem. Phy., 18, 7423−7438, 2018.

Stein, A.F., Draxler, R.R., Rolph, G.D., Stunder, B.J.B., Cohen, M.D. and Ngan, F.: NOAA's HYSPLIT atmospheric transport and dispersion modeling system. Bull. Am. Meteorol. Soc. 96: 2059–2077, 2015.

Tanner, P.A.: Vehicle-related ammonia emissions in Hong Kong. Environ. Chemi. Lett., 7, 37–40, 2009.

Tian, S., Pan, Y., and Wang, Y.: Ion balance and acidity of size-segregated particles during haze episodes in urban Beijing. Atmospheric Research 201, 159–167, 2018.

Walker, J. T., Whitall, D. R., Robarge, W. P., Paerl, H. W.: Ambient ammonia and ammonium aerosol across a region of variable ammonia emission density. Atmos. Environ., 38, 1235–1246, 2004.

Wang, C., Yin, S., Bai, L., Zhang, X., Gu, X., Zhang, H., Lu, Q., Zhang, R.: High-resolution ammonia emission inventories with comprehensive analysis and evaluation in Henan, China, 2006–2016. Atmos. Environ., 193, 11–23, 2018.

Wang, H., Yang, F., Shi, G., Tian, M., Zhang, L., Zhang, L., Fu, C.: Ambient concentration and dry deposition of major inorganic nitrogen species at two urban sites in Sichuan Basin, China. Environ. Pollut., 219, 235–244, 2016.

Wu, S., Dai, L., Wei, Y., Zhu, H., Zhang, Y., Schwab, J. J., Yuan, C.: Atmospheric ammonia measurements along the coastal lines of Southeastern China: Implications for inorganic nitrogen deposition to coastal waters. Atmos. Environ., 177, 1–11, 2018.

Zhang, R., Sun, X., Huang, Y., Shi, A., Yan, J., Nie, T., Yan, X., Li, X.: Secondary inorganic aerosols formation during haze episodes at an urban site in Beijing, China. Atmos. Environ., 177, 275–282, 2018.